JOURNAL OF GEOPHYSICAL RESEARCH, VOL. 101, NO. A6, PAGES 13,483–13,496, JUNE 1, 1996

# The relationship between recurring cosmic ray depressions and corotating solar wind streams at ≤1 AU: IMP 8 and Helios 1 and 2 anticoincidence guard rate observations

I. G. Richardson[1]
Laboratory for High Energy Astrophysics, NASA Goddard Space Flight Center, Greenbelt, Maryland

G. Wibberenz
Institut für Reine und Angewandte Kernphysik, Universität Kiel, Kiel, Germany

H. V. Cane[2]
Laboratory for High Energy Astrophysics, NASA Goddard Space Flight Center, Greenbelt, Maryland

**Abstract.** We examine the detailed relationship between recurrent cosmic ray depressions and corotating high-speed streams in the inner heliosphere near the ecliptic plane using counting rates from anticoincidence guards of instruments on the IMP 8, Helios 1, and Helios 2 spacecraft. These rates indicate the density of >60 MeV/amu ions with reasonable time resolution (~15 min) and high counting statistics. Essentially all corotating streams are accompanied by significant particle depressions. The particle decrease commences most frequently (~63% of events) at the leading edge of the stream which is typically colocated with the stream interface inside the corotating interaction region (CIR). If the depression starts ahead of the interface, there is usually an additional abrupt decrease at the interface. In ~61% of events the onset of the depression is closely associated with the onset of enhanced field turbulence which typically occurs near the stream leading edge. Minimum particle densities are generally found in the vicinity of the maximum solar wind speed in the high-speed stream. The density recovers during the declining phase of the stream. The observations are most consistent with modulation of the cosmic ray density in high-speed streams by the increase in solar wind speed. Enhanced scattering by turbulence in the CIR may also contribute near the onset of the depression, in particular in cases where the decrease commences ahead of the stream interface. The absence of a consistent relationship between the depressions and magnetic field enhancements suggests that localized particle drifts in the enhanced magnetic fields of CIRs do not produce the particle depressions. The observation of a depression is not dependent on the presence of a heliospheric current sheet crossing in the CIR, in contrast to previous reports.

## 1. Introduction

The origin of weak cosmic ray depressions which recur at the solar rotation period is still poorly understood. Their close relationship with corotating high-speed streams [e.g., *Iucci et al.*, 1979] suggests that the deviations from the average solar wind properties associated with these streams play a role, but several processes could contribute. The particles may respond to changes in the solar wind speed (causing variations in convection and adiabatic deceleration), turbulence levels (causing variations in the diffusion tensor), and the magnetic field magnitude (causing variations in particle drifts and the diffusion tensor). Since these parameters all vary across a corotating stream [*Belcher and Davis*, 1971], the response of the cosmic ray density within a stream is likely to be complex. Proposed models of these events have emphasized different processes and hence have produced different predictions of the relationship between the cosmic ray density and stream structure.

A major problem in understanding these depressions and determining which models are most accurate is a lack of detailed observations of their relationship with solar wind structures. Although a large number of studies have been made over 30 years or more, most have used superposed-epoch analyses of neutron monitor data obtained over many events, usually with time resolutions of only ~1 day [e.g., *Lockwood*, 1960; *Duggal and Pomerantz*, 1977; *Iucci et al.*, 1979; *Duggal et al.*, 1981; *Venkatesan et al.*, 1982; *Tiwari et al.*, 1983; *Burlaga et al.*, 1984; *Newkirk and Fisk*, 1985; *Mishra et al.*, 1990; *Singh et al.*, 1990; *Badruddin*, 1993]. Conflicting results have been inferred from such studies. The onset of the particle decrease has been associated with the increase in solar wind speed at the stream leading edge [e.g., *Duggal and Pomerantz*, 1977; *Iucci et al.*,

[1]Also at Department of Astronomy, University of Maryland, College Park.
[2]Also at Physics Department, University of Tasmania, Hobart, Tasmania, Australia.



Paper number 96JA00547.
0148-0227/96/96JA-00547$09.00

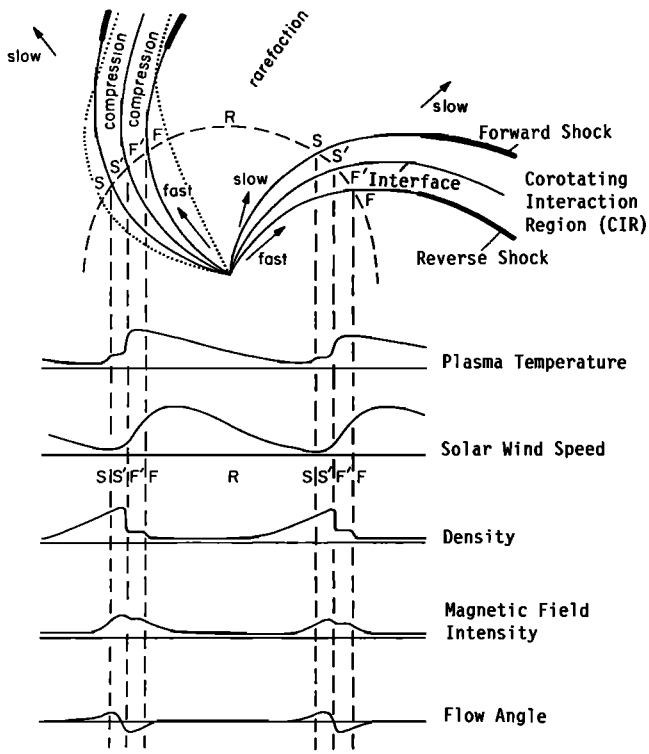


**Figure 1.** Schematic of two high-speed streams corotating with the Sun showing typical changes in solar wind parameters at 1 AU [after *Belcher and Davis*, 1971].

1979], magnetic sector boundaries [e.g., *Fujimoto et al.*, 1981; *Badruddin et al.*, 1985], magnetic field enhancements [e.g., *Murayama et al.*, 1979], and stream interfaces [e.g., *Tiwari et al.*, 1983]. These different conclusions are understandable since these various solar wind structures typically corotate past an observer within ~1 day of the stream leading edge. In addition, some studies [e.g., *Mishra and Agrawal*, 1985; *Shrivastava and Shukla*, 1993] have concluded that corotating streams usually are not associated with cosmic ray decreases. Other studies have used high-energy particle data from spacecraft [e.g., *McCracken et al.*, 1966; *Bukata et al.*, 1968; *Balasubrahmanyan et al.*, 1970; *Morfill et al.*, 1980; *Burlaga et al.*, 1985, 1986]. However, the low counting rates of these data combined with the weak modulations associated with corotating events have generally precluded the detailed examination of individual events. Recurrent decreases have also recently been detected by the Ulysses spacecraft both in the outer heliosphere and at high heliographic latitudes when the spacecraft was continuously immersed in high-speed solar wind from polar coronal holes [*Kunow et al.*, 1995]. It is clearly important to contrast these measurements with observations made in the inner heliosphere near the ecliptic.

Data from the anticoincidence guards of the Goddard Space Flight Center experiment on IMP 8 and the University of Kiel instruments on the Helios 1 and 2 spacecraft can provide such observations. It has only recently been recognized that the guard rate data can indicate the density of >60 MeV/amu ions with high counting rates and without the diurnal variations present in ground-based neutron monitor data. Thus these data are ideal for investigating the detailed relationship between solar wind structures and particle depressions. In several recent papers [e.g., *Cane*, 1993; *Cane et al.*, 1993, 1994; *Cane and Richardson*, 1995; *Richardson and Cane*, 1995b] we have used these data to investigate the relationship between depressions in the cosmic ray density and solar wind structures. These papers focused on cosmic ray depressions associated with transient interplanetary shocks and with material ("ejecta") in the solar wind related to coronal mass ejections (CMEs) at the Sun. In this paper we summarize the properties of 305 particle depressions in the ecliptic associated with corotating high-speed streams at 0.3–1.0 AU from the Sun using IMP 8 and Helios 1 and 2 guard data and concurrent solar wind magnetic field and plasma data. The data are described in section 2. In section 3 we examine the relationship between these depressions and solar wind structure and illustrate several typical events. The observations are discussed in section 4 in terms of models of these events and are summarized in section 5.

## 2. Data

The main data sets for this study are provided by 30-min averages of the count rate from the plastic scintillator anticoincidence guard of the Goddard Space Flight Center medium energy telescope on IMP 8 [*McGuire et al.*, 1986] and 15-min averaged count rates from the anticoincidence guards of the University of Kiel experiments on Helios 1 and 2 [*Kunow et al.*, 1977]. These data give integral rates for ions >60 MeV/amu [*Cane*, 1993; *Cane et al.*, 1993]. During the periods considered in this paper, solar or interplanetary shock-accelerated particle intensities were low and did not contribute significantly to the guard rates. The Helios spacecraft were launched into heliocentric orbits with perihelia of ~0.3 AU and aphelia of ~1.0 AU. To relate the IMP 8 particle observations to solar wind structures, we use solar wind plasma and magnetic field data from the National Space Science Data Center (NSSDC) "OMNI" solar wind database [*Couzens and King*, 1986]. This is a compilation of hourly averaged data from near-Earth spacecraft. The Helios particle data are compared with data from the NSSDC hourly averaged Helios 1 and 2 solar wind tape. This tape includes plasma data from December 15, 1974, to December 24, 1980 (Helios 1), and from January 18, 1976, to March 4, 1980 (Helios 2), and magnetic field data to June 30, 1979, for both Helios spacecraft.

## 3. Observations of Corotating Particle Decreases

### 3.1. Structure of Corotating High-Speed Streams

To place the particle observations in context, Figure 1 shows a schematic of two corotating streams in the ecliptic plane and their characteristic plasma and magnetic field signatures at ~1 AU [after *Belcher and Davis*, 1971]. The interaction between slow and fast solar wind creates a corotating interaction region (CIR) of compressed, heated, plasma at the leading edge of the high-speed stream. The CIR is characterized by enhanced plasma densities and magnetic field intensities together with compressional plasma heating and may be divided into two regions comprising compressed, accelerated slow solar wind (S′ region in Figure 1) and compressed, decelerated fast solar wind (F′ region). The stream interface [*Burlaga*, 1974; *Schwenn*, 1990] which lies at the S′-F′ region boundary inside the CIR is characterized by increases in the solar wind speed and proton temperature, a decrease in plasma density, and a change in the flow angle relative to the radial direction. (The temperature and density variations correspond to the increase

in the specific entropy at the interface discussed by *Intriligator and Siscoe* [1994]). Broad interfaces may originate from steep though continuous transitions in the coronal source structures [*Schwenn*, 1990]. Because of the excess pressure in the CIR the CIR expands into the ambient solar wind. If the expansion speed exceeds the magnetosonic speed, the leading or trailing edge of a CIR may steepen into a forward or reverse shock, respectively (thicker lines in Figure 1). This typically occurs beyond ~2 AU from the Sun [*Smith and Wolfe*, 1977] since the magnetosonic speed decreases with increasing distance from the Sun. For the events to be illustrated below we have indicated the most likely locations of the edges of the CIR based on Figure 1 and the characteristics expected of developing CIR shocks. In particular, the CIR leading edge is expected to be characterized by increases in the plasma density, temperature, and magnetic field intensity together with a westward deviation of the flow direction. The trailing edge is characterized by decreases in the plasma density, temperature, and magnetic field intensity and a return to near-radial flow following an interval with an eastward component. In many streams these features are clearly evident and the CIR edges can be readily identified. In other cases, some or all of these features are weak, making it difficult to infer the extent of the CIR unambiguously.

We have examined 305 corotating streams and the related particle depressions observed at IMP 8, Helios 1, or Helios 2 in 1973–1987. We will concentrate here mainly on the events observed during solar minimum conditions in 1974–1977 because long-lived corotating high-speed solar wind streams were present which originated in isolated near-equatorial coronal holes or equatorward extensions of polar coronal holes [e.g., *Schwenn*, 1990, and references therein] and the Helios and IMP 8 particle observations are most complete during this period. We will first use the multispacecraft data to illustrate the association of recurrent decreases with corotating streams and then examine individual events in order to identify the most usual relationships between decreases and the structure of corotating streams.

### 3.2. Association With Corotating High-Speed Streams

Figure 2 shows Helios 1 and 2 and IMP 8 data for January 18 to March 12, 1976, which illustrate the association of recurrent particle depressions observed in the guard data with corotating high-speed streams. The solar wind speed and guard rate are shown for each spacecraft. To correct for the different experiment characteristics, the IMP 8 guard rates have been normalized to the Helios rates using the relationship $R' = 0.616R + 27.9$, where $R'$ and $R$ are the normalized and observed IMP 8 rates, respectively. This normalization is obtained from a weighted least squares fit to IMP 8 and Helios rates during near-Earth phases of the Helios missions. The dotted vertical lines are spaced at intervals of 1 day. Note that the solar wind data in the fifth panel from the OMNI database are intermittent because of periods when no near-Earth spacecraft was making observations in the solar wind.

The near-ecliptic inner heliosphere during this period was dominated by two high-speed streams. These corotated past Helios 1, then Helios 2, and finally IMP 8 once each 27-day solar rotation. The 1–2 day delays between each spacecraft are consistent with the expected corotation delay. The guard rates are clearly anticorrelated with the local solar wind speed, being depressed by ~1–5% in the high-speed streams. Toward the end of this interval the depressions were apparently deeper at

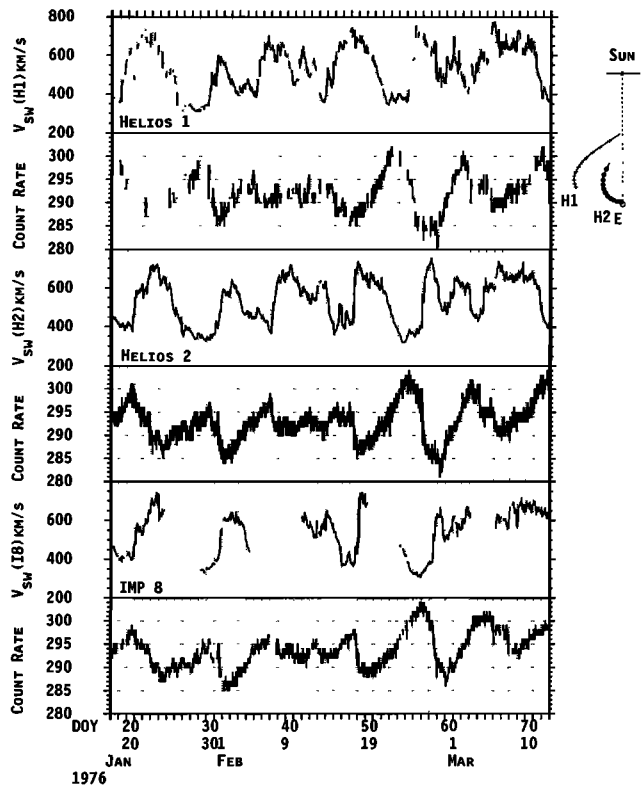


**Figure 2.** Anticoincidence guard count rates and solar wind speed at Helios 1, Helios 2, and IMP 8, for January 18 to March 12, 1976. The IMP 8 count rate has been normalized to the Helios 1 rate in this and the following figures. The spacecraft locations during this interval are indicated. The guard rates are depressed in the high-speed solar wind streams which corotate in turn past Helios 1, Helios 2, and then IMP 8.

the Helios 1 and 2 spacecraft (which were closer to the Sun) than at IMP 8. This observation is qualitatively consistent with a simple model to be presented in section 4 in which the depression is dependent on the number of mean free paths the cosmic rays have to traverse between an outer, undisturbed boundary and the point of observation. This would lead to a larger depression at smaller heliocentric distances. However, some care is necessary in this interpretation since the apparent radial gradient may include contributions from thermal effects in the Helios instruments which are difficult to correct for since no independent check of the >60 MeV/amu ion intensity is available. In addition, the same stream might have been traversed at different latitudes so that different local stream structures were encountered (e.g., see Figure 3.2 of *Schwenn* [1990]).

From examining decreases in the Helios 1 and 2 and IMP 8 data associated with corotating streams, the most striking feature is the anticorrelation between solar wind speed and particle density as illustrated in Figure 2. Figure 3 shows in greater detail three examples in which the depression is particularly closely anticorrelated with the solar wind speed. Note that the depressions commence close to the leading edge of the stream (i.e., the increase in solar wind speed) and extend for several days to the trailing edge of the stream. Maximum depressions occur in the vicinity of the maximum solar wind speed. This type of behavior has been noted before, for example, by *Iucci et al.* [1979] who examined 1-day averages of the neutron

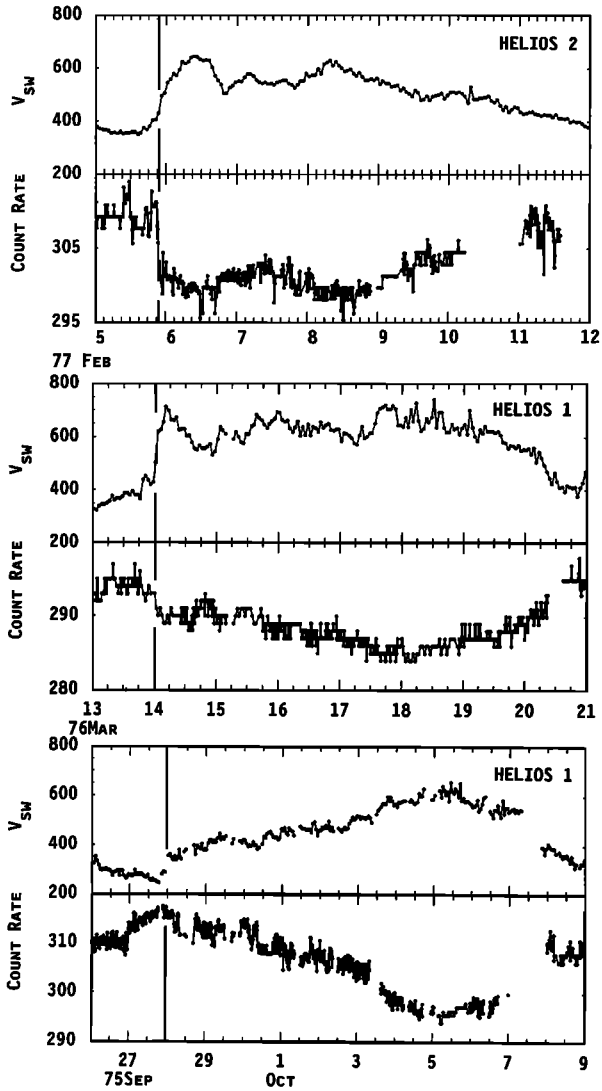


**Figure 3.** Solar wind speed and anticoincidence guard rate for three corotating streams, showing anticorrelations between the solar wind speed and particle density. The vertical line indicates the stream interface.

monitor rate and the solar wind speed for events in 1964–1974. However, the spacecraft data clearly show this relationship on much shorter timescales. For example, the February 1977 event commenced with an abrupt decrease which occurred over a period of only ~1 hour, suggesting that the onset of this decrease was associated with a structure in the solar wind (the stream interface, which is indicated for this and the other events in Figure 3 by a vertical line) which extended over a narrow range of heliolongitude. The relationship between solar wind structures and depression onsets will be discussed further below. *Iucci et al.* [1979] also found that the maximum percentage depression in the cosmic ray density was correlated with the maximum speed inside a stream and with the magnitude of the increase in solar wind speed at the stream leading edge (see also *Newkirk and Fisk* [1985]). We find evidence of similar correlations using the guard rates. Figure 4 examines the relationship between the depth (in percent) of the guard rate depression and the maximum solar wind speed (upper panel) or the increase in solar wind speed at the leading edge of the stream (lower panel) for high-speed streams at IMP 8, Helios 1, or Helios 2 in 1974–1977 at 0.9–1.0 AU (to reduce the effect of variations arising from changing heliocentric distance). The lines indicate least squares fits to the observations, and the corresponding correlation coefficients are indicated. Although there is considerable scatter in the data points, there are positive correlations between the depth of the guard rate depression and both the maximum solar wind speed and the increase in solar wind speed at the stream leading edge, the latter correlation being more significant. The interpretation of this correlation and the scatter in the data points will be discussed further in section 4.

Figure 5 summarizes the percent guard rate depressions in 243 corotating high-speed streams observed by IMP 8, Helios 1, or Helios 2 in 1973–1987 at heliocentric distances 0.9–1.0 AU. The depressions range from ~0 to 8% with a mean of 3.0 ± 1.7%. These depressions are around 2–3 times larger than the neutron monitor decreases (≤2%) reported by *Iucci et al.* [1979] in high-speed streams. A similar ratio between guard rate and neutron monitor percentage decreases was noted in shock-associated decreases by *Cane et al.* [1993] and reflects the lower threshold of the guard counters (~60 MeV/amu versus ~1 GeV/amu). The depressions are also smaller than the ~5–33% shock/ejecta-associated guard count rate

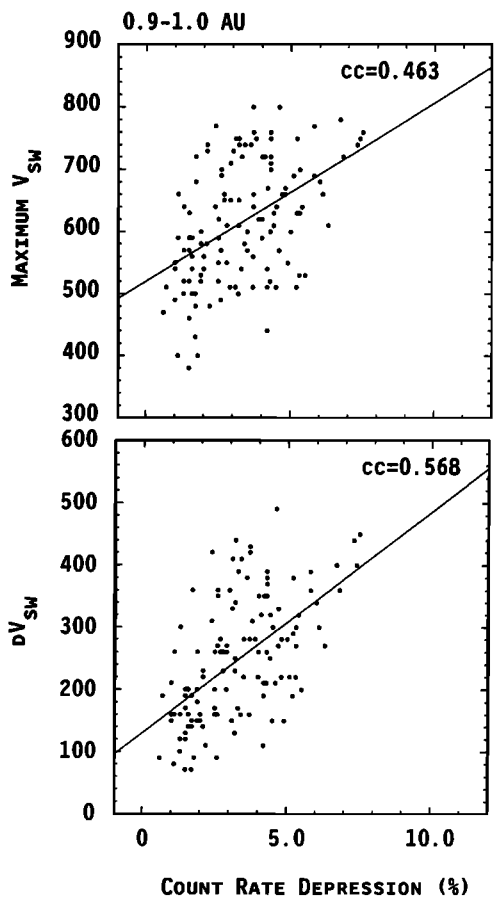


**Figure 4.** The maximum anticoincidence count rate depression in high-speed streams plotted versus (top) the maximum solar wind speed in the stream and (bottom) the increase in solar wind speed from the preceding slow solar wind to the high-speed stream for events at 0.9–1.0 AU. Weak positive correlations are evident.

depressions discussed by *Cane et al.* [1994]. Comparing the depths of the depressions associated with corotating streams in the mid-1970s and mid-1980s solar minima, we find that the mean depressions of 3.4 ± 1.6% and 2.5 ± 1.5%, respectively, do not differ significantly [*Richardson and Cane*, 1995a].

### 3.3. Cosmic Ray Densities in Individual High-Speed Streams and Their Relationship to Stream Structure

Using the guard rate and solar wind data, we are able to examine the relationship between depressions and solar wind structures in detail. To relate the observations with the large-scale structure of CIRs shown in Figure 1, we have examined events in which the stream structure can be reasonably well determined at ≤1 AU.

The depression in Figure 6, observed by Helios 2 on February 17–23, 1976, commenced close to a stream leading edge/interface. The top three panels of Figure 6 show the solar wind magnetic field intensity and polar ($\theta$) and azimuthal ($\Phi$) angles. The next three panels indicate the plasma proton temperature, density, azimuthal flow angle (180° = radial flow), and bulk speed. The next panel shows the 15-min averaged guard count rate. The interval between major tick marks on the vertical axis corresponds to a ~1.7% change in the count rate. The bottom panel shows the value of the sum of the squares of the variances in the magnetic field components ($\sigma B_x^2 + \sigma B_y^2 + \sigma B_z^2$) on the Helios data tape for each 1-hour interval, to give an indication of how the field turbulence levels vary across the stream. The onset of the particle depression is associated with the high-speed stream (HSS) leading edge (i.e., the increase in solar wind speed) and with the stream interface (indicated by the vertical dashed line) which is shown most clearly by the sharp drop in the plasma density inside the CIR (which is identified from the distinct region of enhanced field intensity and plasma density in the vicinity of the stream leading edge). The count rate in the high-speed stream is anticorrelated with the solar wind speed and falls to a minimum close to the CIR trailing edge (at ~2200 UT on February 17 where a developing reverse shock is evident) during a 15-hour interval when the solar wind speed increases. The count rate then recovers over ~5 days during the decline in the solar wind speed. During the period in Figure 6, turbulence levels are greatest inside the CIR on February 17. Although the enhanced turbulence may be expected to contribute to the particle modulation, we note that in this event, the onset of the particle depression occurs significantly (~6 hours) after the onset of enhanced turbulence. Thus the onset of this particular depression appears to be related to the spacecraft crossing the stream interface into the high-speed stream rather than with the enhanced turbulence in the CIR. In addition to this particle depression, two weaker (~0.7%) depressions are evident on February 15–16 associated with brief (<~12-hour duration) high-speed streams. Each stream has a CIR at the leading edge, including the characteristic deviations in the solar wind flow angle.

The Helios 1 data in Figure 7 show two depressions commencing on January 25 and 30, 1975, at increases in the solar wind speed, decreases in density, increases in plasma temperature, and west to east variations in the solar wind flow angle which indicate the interfaces of two corotating high-speed streams. The onset of the January 30 decrease is particularly

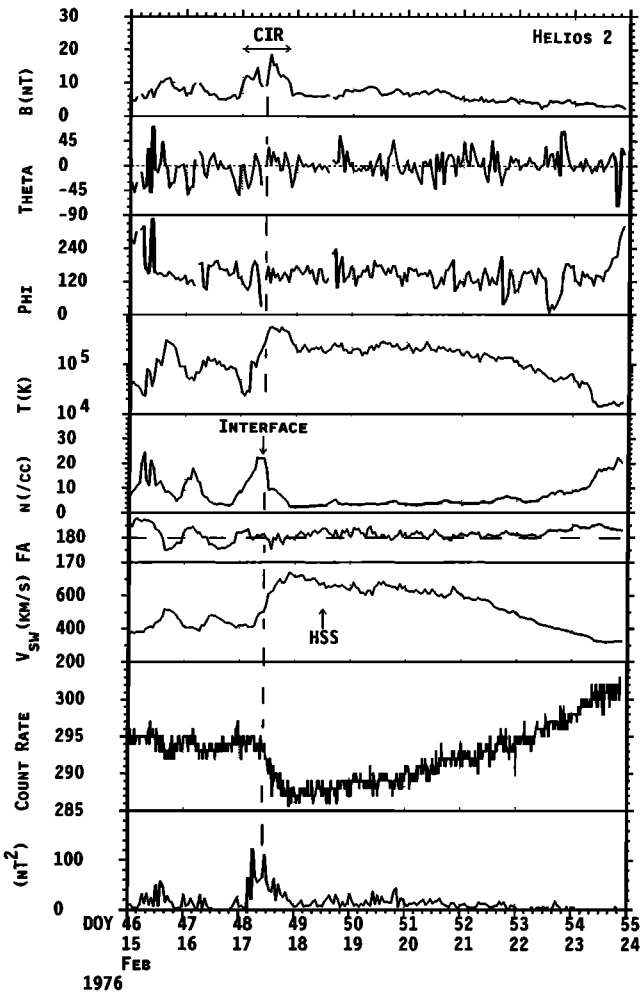


**Figure 6.** Solar wind magnetic field and plasma parameters and guard rates for a high-speed stream (HSS)-associated particle depression at Helios 2 (at 0.87 AU) which commences close to the increase in solar wind speed at the stream leading edge/stream interface and ~6 hours following an enhancement in the magnetic field variance. The two weak depressions on February 15–16 are associated with two brief high-speed streams.

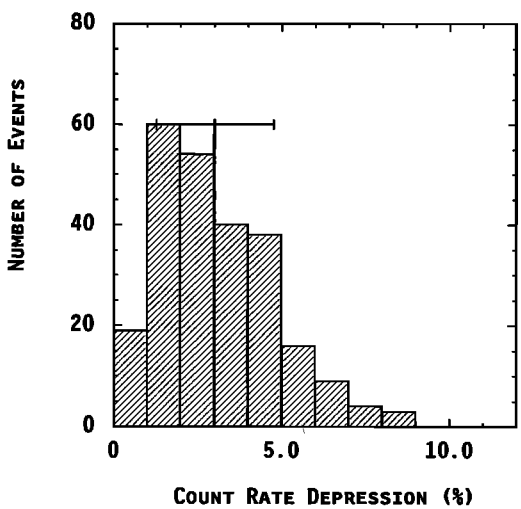


**Figure 5.** Histogram of the anticoincidence guard rate decrease (in percent) for 243 corotating high-speed streams observed at IMP 8, Helios 1, or Helios 2 at 0.9–1.0 AU. The mean depression is 3.0 ± 1.7%.

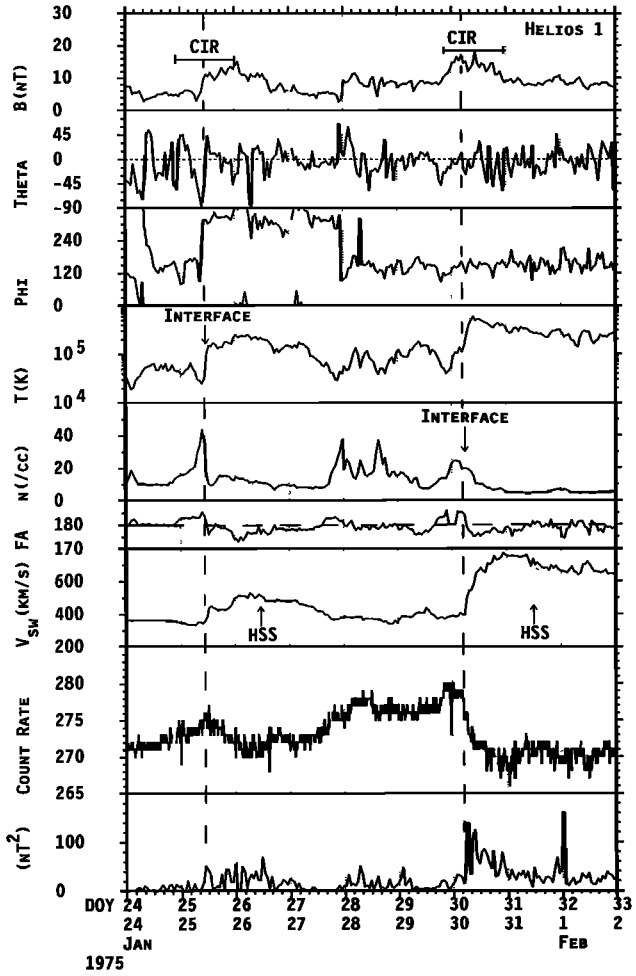


**Figure 7.** Two depressions commencing at stream leading edges/interfaces/increases in magnetic field turbulence levels, observed by Helios 1 at 0.75 AU. Maximum particle densities tend to be observed immediately ahead of the depression inside the CIR.

sharp, the count rate falling by ~1% between 0428–0443 UT and 0458–0513 UT. The boundaries of the CIRs are difficult to identify precisely, though the related increases in plasma density and field intensity in the vicinity of the stream leading edges are evident in Figure 7. In both cases the guard count rate reaches maximum in the CIR at or just preceding the interface and the start of the particle depression. The field turbulence levels increase at the stream interface in both streams, close to the particle depression onset. Note also that while the first depression commences at the leading edge of the magnetic field intensity enhancement associated with the CIR, the second depression (like that in Figure 6) commences well within the CIR magnetic field enhancement. This suggests that there is no consistent association between particle depressions and CIR magnetic field enhancements. Another point to note is that the CIR on January 25 includes a magnetic sector boundary (heliospheric current sheet) crossing, whereas the CIR on January 29–30 does not. The fact that both high-speed streams produced a particle depression is not consistent with the conclusion of *Duggal et al.* [1981] that significant cosmic ray depressions are only produced by CIRs which incorporate the heliospheric current sheet.

We now consider examples of events in which the depression commences ahead of the stream interface. Figure 8 shows a depression at Helios 1 (on June 9–11, 1976) which commences ahead of the stream interface (identified from the increase in proton temperature, decrease in density, and change in the flow angle). The extent of the CIR can be inferred from the region of increased magnetic field intensity, plasma density, and flow angle deviations. The cosmic ray density falls from the leading edge of the CIR and start of the rise in solar wind speed, then decreases more abruptly at the interface to fall to a minimum at the CIR trailing edge which is also the location of maximum solar wind speed. For this event, there is an indication of an initial increase in the field turbulence at the CIR leading edge, close to the time of the depression onset, and a further increase in the vicinity of the stream interface.

The depression in Figure 8 commenced close to the start of the CIR magnetic field enhancement, but consideration of another event commencing ahead of the stream interface suggests that this is not always the case. The decrease at Helios 2 on December 3–5, 1976 (Figure 9), commenced ~12 hours ahead of the interface, yet the magnetic field was only strongly enhanced following the stream interface. It is unclear whether

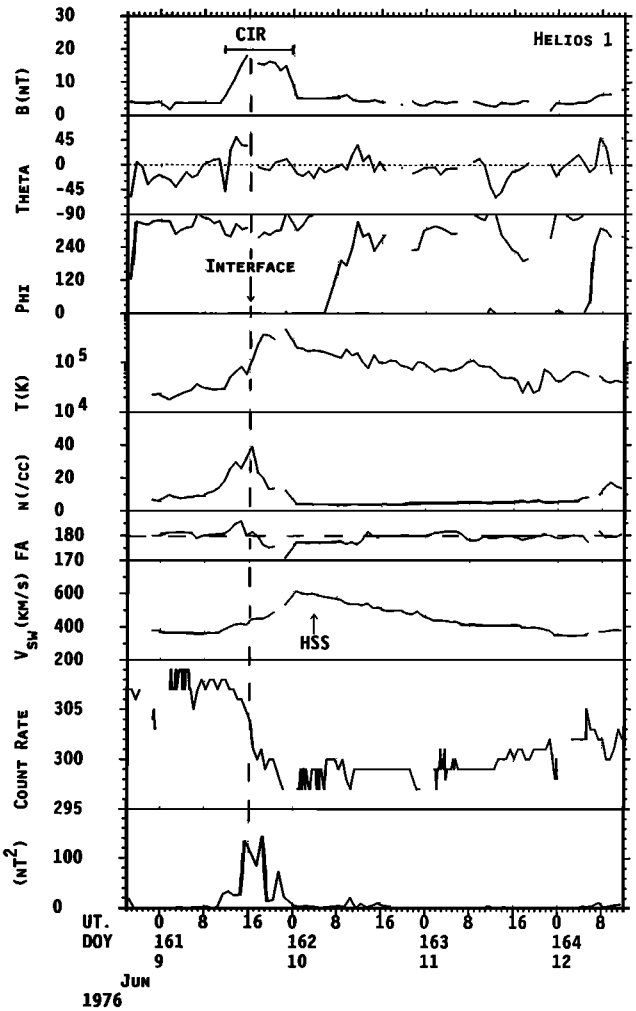


**Figure 8.** A depression commencing before the interface in the vicinity of the probable leading edge of the CIR and an increase in field turbulence, observed by Helios 1 at 0.94 AU. Note the subsequent abrupt decrease at the interface.

the decrease commenced at the leading edge of the CIR since this is difficult to identify precisely. However, the flow angle deflection (FA >180°) and density enhancement during the initial particle decrease suggest that it did occur in a region influenced by the stream-stream interaction, i.e., the CIR. There is only a weak increase in the field turbulence near the start of the depression. As in Figure 8, there is a subsequent abrupt fall in the count rate on crossing the interface which is colocated with the start of the major increase in solar wind speed at the leading edge of the high-speed stream and an increase in turbulence levels.

Although the above events illustrate the types of relationships between solar wind structure and particle depressions which characterize the vast majority of the events studied, as will be discussed further below, a few events do show other relationships. An example, the event of July 21–22, 1975, at Helios 1, is shown in Figure 10. The cosmic ray density minimum occurs in the vicinity of the stream interface and is also associated with a maximum in the magnetic field intensity. An extended depression in the high-speed stream then follows. Events showing maximum depression in the center of the CIR

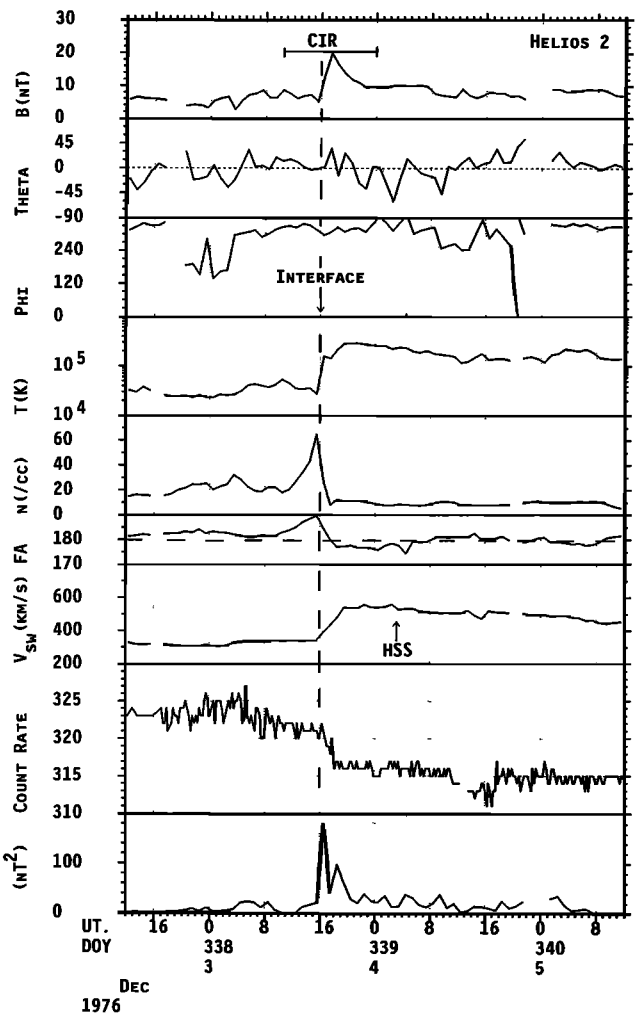


**Figure 9.** Another depression commencing before the interface, observed by Helios 2 at 0.78 AU. Unlike the event in Figure 8, the onset of the decrease is not associated with enhanced magnetic field. Again note the change in the rate of decrease at the stream leading edge/interface.

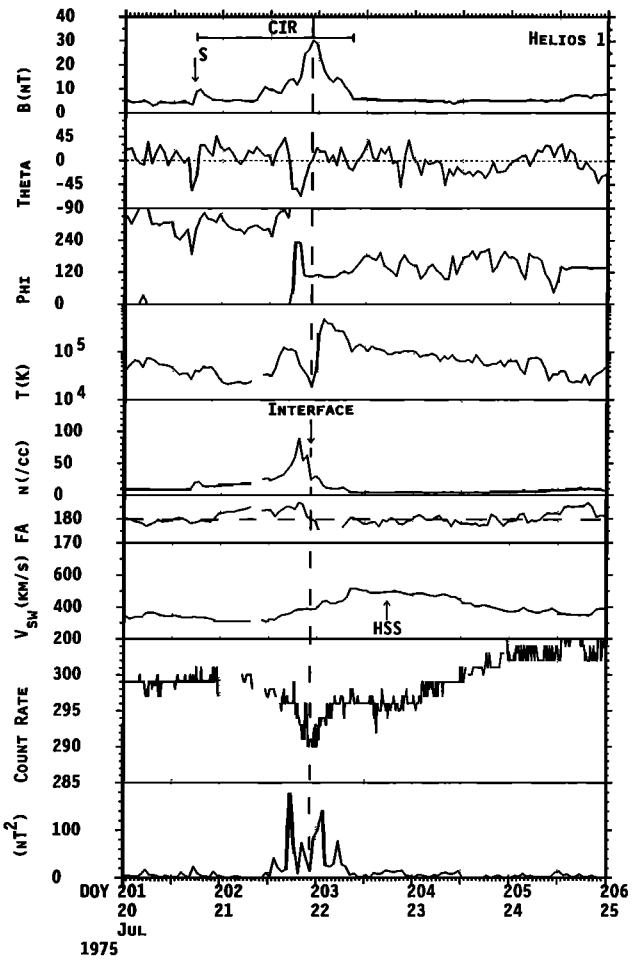


**Figure 10.** A rare example where maximum depression occurs within the CIR, possibly caused by an ejecta in the CIR, observed by Helios 1 at 0.88 AU.

are rare (~5% of events). A possible explanation for this particular event is that the region of cold plasma within the CIR may be an ejecta which produces a local particle depression. The field variance also indicates that this event was unusual in that the level of turbulence increased ~10 hours ahead of the interface, suggesting that increased field turbulence may have contributed to the particle modulation ahead of the interface.

Very few corotating streams have no measurable particle depression. We have found no examples in the IMP 8 and the Helios data during the 1974–1977 solar minimum. Figure 11 shows IMP 8 particle and OMNI solar wind data for one case associated with a corotating stream on July 11–14, 1981, near solar maximum. This stream had a clear CIR at the leading edge, with a stream interface, magnetic field enhancement, and increase in turbulence at the interface, similar to those in other events discussed above, but produced no significant (>0.7%) decrease in the guard rate (or in the University of Tasmania Mount Wellington neutron monitor count rate, not shown here). Overall, we conclude that essentially all corotating high-speed streams produce significant depressions in the >60 MeV/amu ion density.

The above events show similarities and also some differences in the relationship between various solar wind structures and particle depressions. To examine this further, Figure 12 and

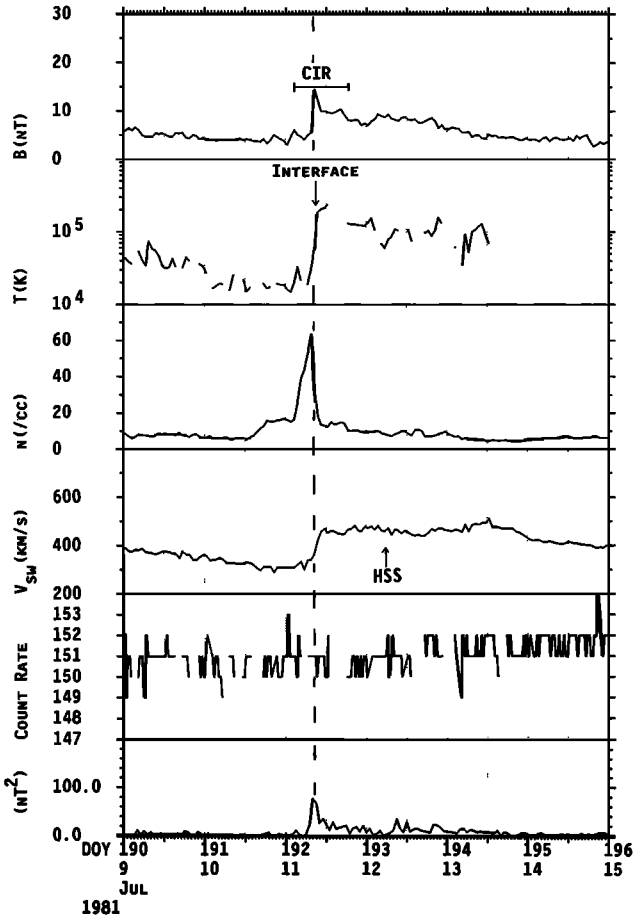


**Figure 11.** A corotating high-speed stream observed at IMP 8 on July 11–14, 1981, which is not accompanied by a significant particle depression.

Table 1 summarize the relationship between depressions and various solar wind features. These features include the stream interface, increase in solar wind speed at the stream leading edge, the beginning and maximum of the CIR-associated magnetic field enhancement, and the onset of magnetic field turbulence as indicated by the field component variance. Each of these panels (the bottom right panel will be discussed separately below) shows a histogram of the time (in 2-hour bins up to ±24 hours) of the depression onset relative to each feature for the Helios 1 and 2 and IMP 8 events where the data are sufficiently complete to allow this interval to be determined. A positive or negative value indicates that the onset commenced after or before, respectively, the solar wind feature was observed. The mean interval is given for each case. Since the number of events varies in each panel, the vertical scale is set to 110% of the maximum number of events in an interval bin to allow the shapes of the distributions to be compared. The most outstanding associations are with the increase in solar wind speed at the stream leading edge (top right panel; mean interval = −1.3 ± 6.9 hours) and with the onset of field turbulence (bottom left panel; mean = 0.7 ± 6.1 hours). Table 1 shows that 63% and 61% of events, respectively, commenced within 3 hours of these features; that is, they were essentially coincident with the onset to within the accuracy with which the onset times can generally be determined from the data.

The top left panel of Figure 12 reflects the conclusion from some of the events illustrated above that the onset of the depression frequently occurs in the vicinity of or ahead of the stream interface. Some 45% of the events commenced within 3 hours of the interface. The distribution is clearly asymmetric, with few events commencing after passage of the interface. In particular, events starting ≥3 hours before the interface outnumber those starting 3 hours or more after the interface by 11 to 1 (Table 1). This asymmetry is reflected by the negative mean interval of −4.8 ± 7.3 hours. The middle left panel shows the time of the depression onset relative to the start of the magnetic field enhancement associated with the CIR. These features coincided to within 3 hours in 44% of events. The distribution is broad and asymmetric, with a predominance of events commencing after the start of the magnetic field enhancement (Table 1) resulting in a mean interval of 3.9 ± 7.2 hours. This asymmetry arises because depressions tend to start at or following the start of the field enhancement associated with the CIR (in particular in the vicinity of the stream interface/leading edge in the middle of the CIR). The middle right panel shows the onset time relative to the time of maximum magnetic field in the vicinity of the CIR. Around 34% of events commence within 3 hours of this feature. There is a peak at the time of field maximum and an asymmetrical distribution in which events commencing ahead of the field maximum outnumber those commencing afterward by ~9:1, giving a mean interval of −5.4 ± 7.4 hours. Since peak fields are likely to occur near the interface in the middle of the CIR, the asymmetry reflects the distribution relative to the interface in the top left panel. Overall, our conclusion is that the increase in solar wind speed organizes the onset times of corotating events reasonably well. This is also frequently colocated with the stream interface and the onset of enhanced field turbulence and may be accompanied by the start of a magnetic field intensity enhancement or maximum magnetic fields, as is evident in the events discussed above. There is also evidence of ordering by the onset of magnetic field turbulence.

The bottom right histogram in Figure 12 is slightly different in that it shows the time of maximum depression (rather than depression onset) relative to the trailing edge of the CIR (i.e., the developing reverse shock), where this interval can be inferred. (The binning here is in 4-hour intervals.) The most likely location for the maximum depression (~30% of events) is at the CIR trailing edge, though it can lie several tens of hours after the CIR in the high-speed stream. For 89% of the events the maximum depression occurs at or following the trailing edge of the CIR, so it is rarely observed inside the CIR. The mean interval is 19 ± 33 hours.

## 4. Discussion

We have used anticoincidence guard rate data from three spacecraft to study cosmic ray density depressions associated with 305 corotating high-speed streams at 0.3–1.0 AU. We find that

1. Essentially all corotating high-speed streams are accompanied by cosmic ray depressions. The mean >60 MeV/amu ion depression observed in 243 corotating high-speed streams at 0.9–1.0 AU is 3.0 ± 1.7%, and depressions in individual streams range from ~0 to 8%.

2. Typically, the solar wind speed and depth of the depression in individual streams are anticorrelated. The recovery phase of the depression is usually more gradual than the onset phase and extends over several days to the trailing edge of the

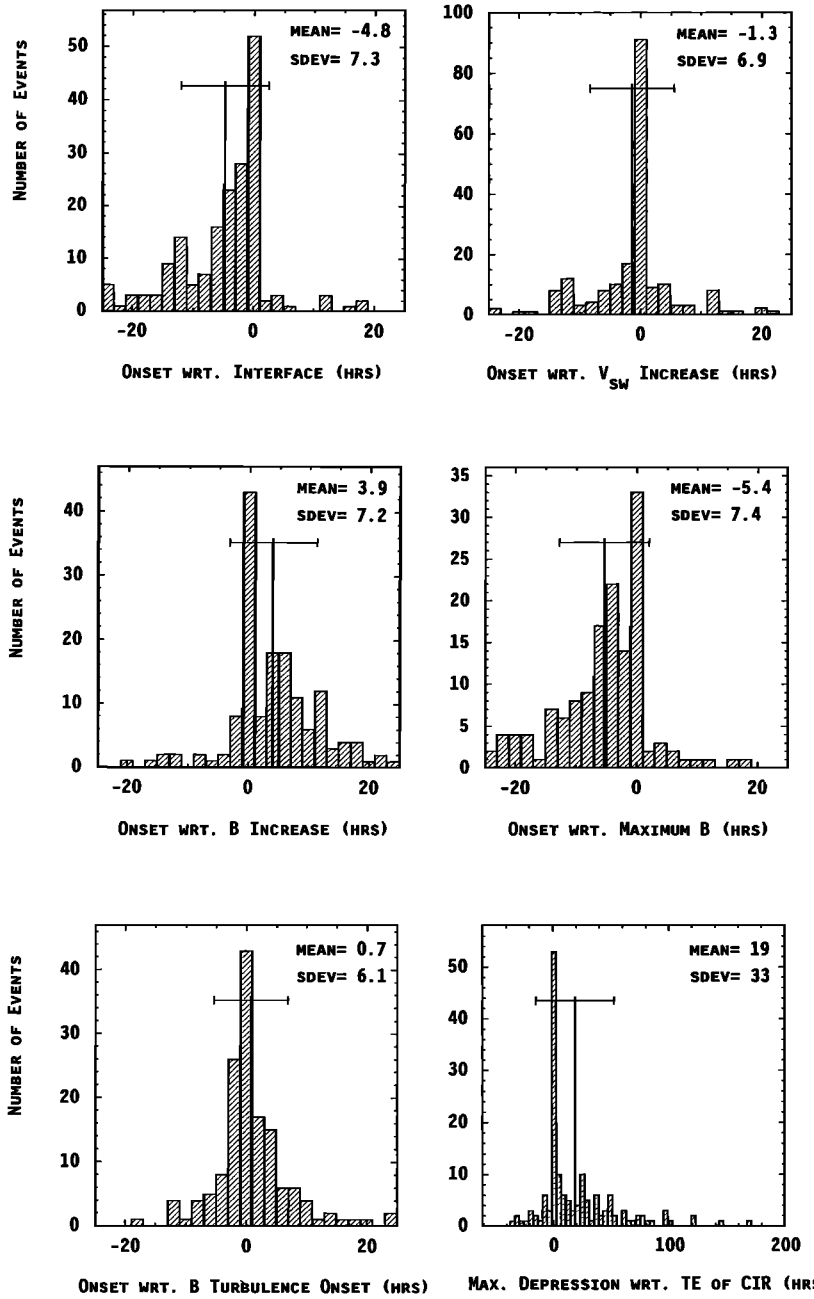


**Figure 12.** Histograms showing the onset time of Helios 1 and 2 and IMP 8 particle decreases with respect to the stream interface, the increase in solar wind speed at the leading edge of a high-speed stream, the start of the magnetic field enhancement associated with the CIR, the time of maximum magnetic field inside the CIR, and the onset of enhanced magnetic field turbulence. A negative (positive) time indicates that the onset started ahead of (after) the solar wind structure. The closest associations are with the increase in solar wind speed and onset of magnetic field turbulence. The bottom right panel shows the time of maximum particle depression relative to the trailing edge of the CIR (location of the developing reverse shock).

stream. Depression maximum occurs close to the time of maximum solar wind speed, which is most frequently located at the trailing edge of the CIR (where a developing reverse shock is often evident), but may occur several days later. Considering all the streams, the maximum depression is correlated both with the jump in speed from slow solar wind to high-speed stream and with the maximum speed in the stream.

3. The onset of the particle depression occurs most frequently at (i.e., within 3 hours of) the increase in solar wind speed at the leading edge of the high-speed stream (63% of events) or at the increase in magnetic field turbulence generated by the stream-stream interaction which is usually also associated with the increase in solar wind speed (61% of events). The onset is located at the stream interface in ~45% of events. In events where the decrease commences prior to the interface, generally in the vicinity of the leading edge of the CIR (developing forward shock) if this can be identified, there is usually a subsequent abrupt decrease in the count rate at the

**Table 1.** Time of Particle Depression Onset Relative to Solar Wind Structures

| Structure | No. of Events | Percentage of Events with Time Difference | | | Ratio of No. of Events Commencing ≥3 Hours Before and After Structure |
|---|---|---|---|---|---|
| | | ≤3 hours | ≤6 hours | ≤12 hours | |
| $V_{SW}$ increase | 198 | 63% | 73% | 89% | 2.2:1 |
| Turbulence onset | 152 | 61% | 78% | 91% | 0.8:1 |
| Interface | 187 | 45% | 66% | 81% | 11:1 |
| $\|B\|$ Increase | 155 | 44% | 63% | 85% | 0.2:1 |
| Maximum $B$ | 149 | 34% | 61% | 79% | 9:1 |

interface. Rarely (~5% of events), maximum depression occurs inside the CIR.

4. In some cases, cosmic ray enhancements are attained inside the CIR and immediately ahead of a depression.

5. There is no consistent relationship between the CIR magnetic field enhancement and the particle decrease. The start of the decrease may occur at the leading edge of the field enhancement or well inside it.

6. Depressions are observed irrespective of whether the CIR includes a heliospheric current sheet crossing.

7. The depths of particle depressions during the mid-1980s solar minimum are not significantly different on average from those during the mid-1970s solar minimum.

Some of the properties of corotating particle depressions described above are consistent with those inferred previously using superposed-epoch analyses of neutron monitor data. For example, the observation of maximum cosmic ray densities immediately ahead of high-speed streams is consistent with the 1-day averaged superposed-epoch neutron monitor observations of *Fujimoto et al.* [1981] (though these observations were specifically keyed to sector boundaries rather than high-speed streams) and those of *Duggal and Pomerantz* [1977]. Anticorrelations between solar wind speed and particle decreases have also been previously noted using neutron monitor data [e.g., *Duggal and Pomerantz*, 1977; *Iucci et al.*, 1979].

In light of these observations we briefly consider whether various models to explain cosmic ray decreases associated with corotating solar wind streams are consistent with the observations. Because the cosmic rays may respond to changes in the solar wind speed, turbulence, and magnetic field intensity and these may occur remotely from the spacecraft, the resulting influence on the cosmic ray density in the inner heliosphere is likely to be complex. However, the observations allow us to infer which processes may be more important.

The clear anticorrelation between particle density and solar wind speed within high-speed streams suggests that the enhanced convection of cosmic rays from the inner heliosphere may be a major process producing corotating particle depressions in high-speed streams. We can illustrate that this mechanism may account for these anticorrelations and for depression maxima which occur in the vicinity of the solar wind speed maximum in the stream, sometimes well away from the stream leading edge, using a steady state diffusion-convection model which includes adiabatic deceleration and longitudinal variations. The force-field approximation for galactic cosmic ray modulation is given by

$$CUV_{SW} = D_r(\partial U/\partial r) \tag{1}$$

where $C$ is the Compton-Getting factor, $U$ is the cosmic ray density, $V_{SW}$ is the solar wind speed, and $D_r$ is the radial diffusion coefficient. To estimate the value of $C$, we take the characteristic energy of the guard detectors as 1 GeV, which is close to the median energy for an integral detector responding to cosmic ray depressions [*Lockwood et al.*, 1991]. In this case, $C = 1.3$ [*Forman and Gleeson*, 1975] and is taken to be independent of azimuth. Suppose $U(r)$ is independent of azimuth outside a distance $r_2$. The density at a smaller distance from the Sun, $r_1$, will then be

$$U(r_1) = \exp(-3\ CV_{SW}N_1/c)U(r_2) \tag{2}$$

where $N_1$ is given by

$$N_1 = \int_{r_1}^{r_2} \frac{dr}{\lambda_r}. \tag{3}$$

This parameter essentially corresponds to the number of mean free paths between $r_1$ and $r_2$, though it should be remembered that $\lambda_r$ is the effective radial mean free path which depends on the parallel and perpendicular diffusion coefficients according to

$$\lambda_r = \cos^2\phi\lambda_{\parallel} + \sin^2\phi\lambda_{\perp}. \tag{4}$$

*Morfill et al.* [1979] predict that beyond 1 AU, the scattering mean free path in the trailing edge of a high-speed stream is essentially independent of azimuth (see their Figures 7 and 8). In this case, $V_{SW}$ is the only quantity variable with longitude, and differentiation of (2) leads to

$$\partial U/U = -3\ CV_{SW}N_1\ \partial V_{SW}/c \tag{5}$$

This relationship is evidently consistent with the observed general anticorrelation between the increase in solar wind speed and fractional decrease in cosmic ray density. The straight-line fit to the data in the bottom panel of Figure 4 suggests that $N_1 = 21.2$. To check whether this value is consistent with estimates of $\lambda_r$, we need to make reasonable assumptions for $r_2$ and the radial dependence of $\lambda_r$. A plausible value for $r_2$ is 10 AU since *Burlaga et al.* [1983] found that the azimuthal structure of individual solar wind streams structures is greatly diminished at 8.5 AU. Also, the decrease in the intensity of low-energy particle enhancements associated with CIRs between 5 and 10 AU [e.g., *Van Hollebeke et al.*, 1978] suggests that the influence of individual streams is reduced at this distance. Using $r_2 = 10$ AU and assuming first that $\lambda_r$ is independent of radial distance [e.g., *Müller-Mellin and Wibberenz*, 1995] give a radial mean free path of ~0.4 AU for the above value of $N_1$. Alternatively, if $\lambda_r$ is proportional to $r^{0.4}$ [*Hamilton*, 1977], this implies that $\lambda_r$ (1 AU) = 0.23 AU. These estimates are not inconsistent with estimates of $\lambda_r$ (1 AU) = 0.25 AU ($\lambda_{//} = 0.5$ AU) for 1-GeV protons [e.g., *Bieber et al.*, 1994], in particular considering that $\lambda_r$ is likely to be a function of particle rigidity and the exact rigidity response of the guard

detectors is not well known. Thus the observations are at least consistent with the conclusions from this simple model with realistic particle mean free paths. In the context of this model the deviations of the points in the bottom panel of Figure 4 from the straight line may arise because of variations in the value of $\lambda_r$ from stream to stream related to differences in the degree of scattering [*Wanner and Wibberenz*, 1993]. The model also explains the correlation between the size of the depression and the solar wind speed in the trailing edges of individual streams as well as gradual particle decreases during extended stream leading edges such as that shown in the bottom panel of Figure 3. For this event the slow rise in the speed and associated decrease in the particle density together with application of (2)–(4) also happen to give $N_1 = 21.2$ so these observations are again consistent with the model using the values of $\lambda_r$ discussed above in relation to the bottom panel of Figure 4.

The assumption of azimuthally independent scattering within a high-speed stream in the above model is unlikely to be correct in the vicinity of the leading edge of the stream. Analyses of field and plasma data from various spacecraft within and beyond 1 AU from the Sun [e.g., *Belcher and Davis*, 1971; *Morfill et al.*, 1979; *Richardson*, 1985; *Badruddin*, 1993; *Tsurutani et al.*, 1995] and the observations presented above indicate that turbulence is generally greatest in the vicinity of the CIR, in particular in the region between the interface and CIR trailing edge where the solar wind speed rises, and tends to follow the plasma temperature profile shown in Figure 1. Thus we might expect some modification to the simple particle density–solar wind speed anticorrelation in the vicinity of the stream leading edge. The close association discussed above between enhanced field turbulence and a majority (>60%) of particle depression onsets suggests that enhanced field turbulence may play a role in the onset of some decreases.

The suggestion that turbulent magnetic fields generated by the stream-stream interaction are responsible for producing corotating decreases, by depressing the cosmic ray density on field lines in the fast stream which intersect the interaction region, was made by *McCracken et al.* [1966]. In their model the particle depression at 1 AU commences at the leading edge of the interaction region (which they associated with an increase in magnetic field intensity). This is consistent with events in which the depression commences well ahead of the interface, in particular at the leading edge of the CIR such as that in Figure 8, but not with the larger number of events in which the decrease commences in the vicinity of the stream leading edge within CIRs. The variations in the magnetic field turbulence have also been incorporated in the model of *Morfill et al.* [1979]. This model predicts that the cosmic ray density should peak within the CIR in the vicinity of the stream interface and then fall rapidly in the fast stream following the stream interface before recovering more slowly during the decay phase of the stream, in general agreement with our observations. The peak inside the leading edge of the CIR arises in this model because the "most probable" turbulence direction vector is more closely aligned with the magnetic field in this region and this more than counteracts the effect of increased turbulence on radial diffusion. We also note that *Kunow et al.* [1995] find in the outer heliosphere near the ecliptic that the particle depressions observed by the Ulysses spacecraft generally commence at the leading edge of the CIR, i.e., ahead of the stream interface, in contrast to the case in the majority of events observed in the inner heliosphere. One possibility is that since the forward shock is typically better developed in the outer heliosphere than in the inner heliosphere, local levels of turbulence inside the leading edge of the CIR may be higher than in the inner heliosphere, causing greater modulation.

*Morfill et al.* [1980] compared the model of *Morfill et al.* [1979] with one in which scattering and consequent cosmic ray modulation occur only in the CIR and in the region in the outer heliosphere where CIRs associated with separate streams are expected to merge into one disturbed region. Elsewhere, scatter-free propagation was assumed, and the particle density was essentially determined by the modulated density at the point where a field line intersects the CIR in the outer heliosphere. According to this model the particle depression should commence several days ahead of the leading edge of the CIR, reach greatest depth in the vicinity of the stream interface (since particles on these field lines remain inside the CIR and so are subject to maximum modulation), and recover to a local maximum several days later during the decay phase of the high-speed stream before falling again toward the CIR of the next stream. These expectations are not consistent with the majority of the events studied since the depression does not start ahead of the CIR, there is no minimum in the CIR in the vicinity of the interface, and maximum densities are not found during the stream decay phase. Thus we agree with the overall conclusion of *Morfill et al.* [1980] that observations of cosmic ray depressions associated with high-speed streams are more consistent with an interplanetary diffusion model wherein scattering is determined by the solar wind and magnetic field microstructure everywhere in the heliosphere.

Another effect which may occur near the leading edge of the stream was discussed by *Barouch and Burlaga* [1975, 1976]. They suggested that enhanced drifts of particles out of regions of enhanced fields in CIRs might produce the depressions associated with high-speed streams. On the basis of our observations it is unlikely that this mechanism can make a major contribution to particle depressions since there is little evidence of a consistent spatial/temporal relationship between CIR magnetic field enhancements (for example, the start of the field increase or its maximum) and the particle depressions. We also note two other studies of the relationship between the interplanetary magnetic field and recurrent particle depressions which do not appear to be supported by our observations. *Murayama et al.* [1979] concluded that magnetic field enhancements associated with corotating high-speed streams in which the field retains a Parker spiral configuration do not produce cosmic ray depressions. However, our observations clearly indicate that such magnetic field enhancements (e.g., the events illustrated in this study) are accompanied by cosmic ray depressions. Also, *Duggal et al.* [1981] concluded that significant cosmic ray depressions (observed by neutron monitors) were only produced by CIRs which incorporate the heliospheric current sheet. Examining our events, we see no evidence for such an effect. Decreases are certainly evident in individual streams which do not have a current sheet crossing in the CIR (e.g., Figure 6; the second event in Figure 7; Figures 8 and 9). Also, the mean depression for events within which a current sheet crossing occurred within one day of the start of the decrease is 3.2 ± 1.9% compared to 2.5 ± 1.6% for events without crossings, there being no significant difference in these values. We also find no significant difference in the correlation between the size of the decrease and solar wind speed increase for each group of events. Thus we conclude that the depression depth is not strongly dependent on the presence or absence of a current sheet crossing in the CIR.

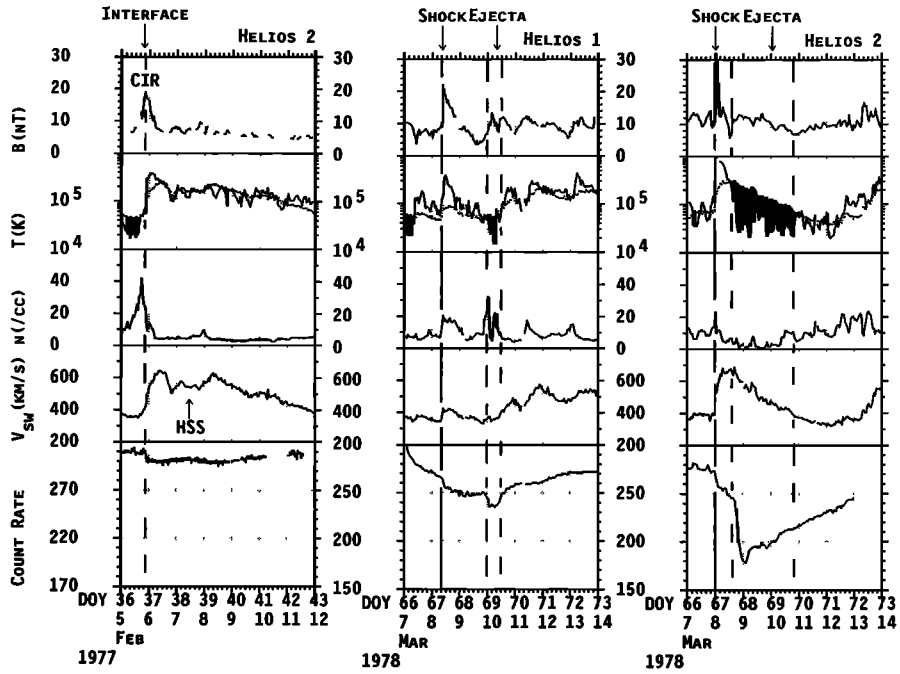


**Figure 13.** Comparison of anticoincidence guard rate depressions (left) at Helios 2 associated with a corotating high-speed stream, (center) following a shock at Helios 1 in which the ejecta is only grazed well after shock passage, and (right) following a shock at Helios 2 showing the deep local depression in the ejecta. The different characteristics of the depressions are evidently related to the different solar wind structures encountered.

*Kota and Jokipii* [1991] have investigated the influence of CIRs on the global cosmic ray distribution using a very complete three-dimensional model incorporating parallel and perpendicular diffusion, drift, convection, and adiabatic deceleration. The effect of the CIRs is to produce particle decreases which commence in the vicinity of the start of the CIR magnetic field enhancement and reach maximum depression at the CIR trailing edge (i.e., in the vicinity of the developing reverse shock). This contrasts with our observations which suggest the absence of a one-to-one relationship between magnetic field enhancements and depressions (with a caveat that the results of *Kota and Jokipii* [1991] were calculated for 2-GeV protons at 10 AU rather than >60 MeV/amu ions at 1 AU). The reason for the close association between CIRs and particle depressions in the *Kota and Jokipii* [1991] model lies in the fact that the diffusion coefficient is scaled as $1/B$ so that the modulation is caused by the increased scattering assumed to be present in the CIR [*Kota and Jokipii*, 1991]. We note that away from CIRs in the trailing edges of high-speed streams where B (and hence the mean free path) changes little with azimuth in their model, the anticorrelation between solar wind speed and particle density discussed above in relation to our observations is evident in their model. The model predicts that particle depressions should be ~50% smaller for solar magnetic field polarity $A > 0$ than for $A < 0$. However, our observations do not indicate any significant dependence on $A$, giving mean depressions of 3.4 ± 1.6% for IMP 8 events in the mid-1970s solar minimum ($A > 0$) and 2.5 ± 1.5% in the mid-1980s solar minimum ($A < 0$) [*Richardson and Cane*, 1995a]. The large errors reflect the wide stream-to-stream variation in the depressions which evidently predominates over effects due to drifts in large-scale magnetic fields.

It is interesting finally to compare the depressions associated with corotating streams with those related to interplanetary shocks. Figure 13 compares three representative particle depressions using similarly scaled axes in order to emphasize the similarities and differences in the depressions. In addition to parameters shown in previous figures we compare the measured proton temperature ($T_p$) with the temperature expected for normal solar wind expansion ($T_{ex}$) [*Lopez*, 1987, and references therein; *Cane and Richardson*, 1995; *Richardson and Cane*, 1995b] shown by a dotted line. This comparison is useful in identifying regions of abnormally low temperature plasma which are generally associated with ejecta or with the heliospheric plasma sheet (HPS, or streamer belt) which envelopes the heliospheric current sheet [*Richardson and Cane*, 1995b]. Shaded regions in the second panel denote $T_p/T_{ex} < 0.5$. The left-hand panel shows a particle decrease at Helios 2 associated with a corotating stream (note that the decrease onset is located at the stream leading edge/stream interface). The center panel shows a shock-associated depression at Helios 1 in March 1978 in which the probable ejecta (indicated by low-temperature plasma) was only briefly encountered. The major contribution to the depression is apparently due to the effect of connection to a region of enhanced solar wind speed and the postshock turbulence, with an additional local depression in the ejecta [*Cane et al.*, 1994]. (The enhanced, decaying particle fluxes at the beginning of this period are associated with a solar particle event and return to cosmic ray background levels by the time of shock passage.) The right-hand panel shows observations of this same shock at Helios 2. This spacecraft encountered the ejecta, indicated by strongly depressed proton temperatures, a few hours after shock passage [*Cane et al.*, 1994]. In this case the depression has two steps, the first at the shock

and related to the postshock turbulence and the second, more abrupt decrease at entry into the ejecta. The decrease in the ejecta may arise from the closed magnetic structure of the ejecta which particles can only enter by cross-field diffusion [*Cane et al.*, 1995]. This event has the form of the classic rapid-onset Forbush decrease, which our previous studies have demonstrated is generally only observed if the ejecta is encountered following the shock. Thus we emphasize that it is the encounter with the ejecta that produces the large, abrupt depression which is the major difference between corotating depressions and Forbush decreases. Therefore studies which attempt to relate the differences between corotating stream-associated depressions and Forbush decreases in terms of differences in one solar wind parameter (such as $V_{SW}$, $B$, or $\sigma B$) will not be successful since they do not take into account the fact that the solar wind structures present are fundamentally different. It is interesting that the decreases produced by the corotating stream in the left-hand panel and by the shock effect in the center panel are similar in magnitude. This may be fortuitous, however, because the spatial structure and temporal development of the affected region, and connection of the observer to this region, may be different. We also note that the magnetic field intensity has no obvious consistent relationship with the cosmic ray depressions. The start of the depression follows a field intensity peak in the left-hand panel and is associated with a sharp increase in magnetic field in the center panel and for the first step of the decrease in the right-hand panel. The deep depression in the right-hand panel, associated with the ejecta, has no related major increase in the magnetic field intensity. It is evident that the simple empirical relationship $dI/dt = -D(B/B_p - 1)$ between enhancements in the magnetic field intensity above the mean Parker value ($B_p$) and the cosmic ray density ($I$) which has been derived from depressions in the cosmic ray intensity observed at spacecraft at large heliocentric distances [*Burlaga et al.*, 1985] and used to model cosmic ray depressions in the outer heliosphere [e.g., *Burlaga et al.*, 1993] does not appear to be followed by our higher time resolution data at $\leq$1 AU. The essential reason is that this relationship is only valid beyond 10 AU where global merged interaction regions dominate the modulation [*Burlaga et al.*, 1985]. The relationship does not differentiate between the different solar wind structures which produce the particle depressions (as in Figure 13) in the inner heliosphere. Hence we should not expect it to hold rigorously for our observations.

## 5. Summary

Our observations of cosmic ray depressions associated with corotating high-speed streams show the following features:

1. A majority (~63%) of these depressions commence close to the leading edge of the associated high-speed stream, with an excellent anticorrelation between the cosmic ray density and $V_{SW}$ in the trailing edges of individual high-speed streams. This is consistent with a simple model in which cosmic ray modulation is determined by the variation in the solar wind speed together with a mean free path which varies little with longitude. The anticorrelation is also evident between the maximum depression and solar wind speed in a group of streams. However, the correlation is weaker possibly because the degree of scattering may vary from stream to stream.

2. There is also a close association between the depression onset and the start of enhanced magnetic field turbulence, as indicated by the field component variances, in ~61% of the events. This association may occur because there is a general increase in turbulence levels at stream leading edges and because locally enhanced particle scattering may contribute to the particle modulation. In particular, increased scattering may play a role in cases where the depression commences before the increase in solar wind speed. However, in general, at $\leq$1 AU, enhanced turbulence (in particular in the vicinity of the CIR) does not seem to play a large role in the phase of the maximum depression since we generally do not observe any major depression in addition to that associated with the solar wind speed. At Ulysses [*Kunow et al.*, 1995], observations suggest that particle decreases generally commence close to the CIR leading edge. This may occur when turbulence close to the CIR forward shock (or the region which is going to develop into the forward shock in the outer heliosphere) is sufficiently high.

3. There is no consistent relationship between CIR-associated magnetic field enhancements at stream leading edges and the particle decrease, indicating that drifts away from regions of enhanced magnetic fields do not play a major role in producing these decreases.

4. Depressions are observed irrespective of whether the CIR includes a heliospheric current sheet crossing.

5. Recurrent particle depressions during the mid-1980s solar minimum are not significantly different on average than those during the mid-1970s solar minimum. The large stream-to-stream variations obscure the possible influence of drifts in large-scale magnetic fields which are expected to be dependent on the direction of the solar magnetic field.

6. In some events, there is a local maximum in the cosmic ray density just ahead of the depression inside the CIR. The most reasonable explanation seems to come from the results of *Morfill et al.* [1979] in which the distribution of wave vectors leads to reduced scattering in this part of the CIR.

**Acknowledgments.** We acknowledge the use of data from the tape of Helios merged hourly averaged field (P.I. F.M. Neubauer) and plasma (P.I. H. Rosenbauer) data (NSSDC ID 74-097A-09B) and from the OMNI on-line database, all provided by the National Space Science Data Center. HVC was supported at GSFC by a contract with the Universities Space Research Association. The work of IGR was supported by NASA grant NGR 21-002-316.

The Editor thanks R. B. McKibben and C. W. Smith for their assistance in evaluating this paper.

## References

Badruddin, Cosmic ray modulation and high-speed solar wind streams of different origin, *Proc. Int. Conf. Cosmic Rays 23rd*, *3*, 727, 1993.

Badruddin, R. S. Yadav, and N. R. Yadav, Intensity variation of cosmic rays near the heliospheric current sheet, *Planet. Space Sci.*, *33*, 191, 1985.

Balasubrahmanyan, V. K., E. C. Roelof, R. P. Bukata, and R. A. R. Palmeira, Corotating modulations of cosmic ray intensity detected by spacecrafts (sic) separated in solar azimuth, *Proc. Int. Conf. Cosmic Rays 11th, Acta Phys. Acad. Sci. Hung.*, *29*, suppl. 2, 31, 1970.

Barouch, E., and L. F. Burlaga, Causes of Forbush decreases and other cosmic ray variations, *J. Geophys. Res.*, *80*, 449, 1975.

Barouch, E., and L. F. Burlaga, Three-dimensional interplanetary stream magnetism and energetic particle motion, *J. Geophys. Res.*, *81*, 2103, 1976.

Belcher, J. W., and L. Davis, Large amplitude Alfvén waves in the interplanetary medium, 2, *J. Geophys. Res.*, *76*, 3534, 1971.

Bieber, J. W., W. H. Matthaeus, C. W. Smith, W. Wanner, M.-B. Kallenrode, and G. Wibberenz, Proton and electron mean free paths: The Palmer consensus revisited, *Astrophys. J.*, *420*, 294, 1994.

Bukata, R. P., K. G. McCracken, and U. R. Rao, A comparison of

corotating and flare-initiated Forbush decreases, *Canadian J. Phys.*, *46*, S994, 1968.
Burlaga, L. F., Interplanetary stream interfaces, *J. Geophys. Res.*, *79*, 3717, 1974.
Burlaga, L. F., R. Schwenn, and H. Rosenbauer, Dynamical evolution of interplanetary magnetic fields and flows between 0.3 AU and 8.5 AU: Entrainment, *Geophys. Res. Lett.*, *10*, 413, 1983.
Burlaga, L. F., F. B. McDonald, N. F. Ness, R. Schwenn, A. J. Lazarus, and F. Mariani, Interplanetary flow systems associated with cosmic ray modulation in 1977–1980, *J. Geophys. Res.*, *89*, 6579, 1984.
Burlaga, L. F., F. B. McDonald, M. L. Goldstein, and A. J. Lazarus, Cosmic ray modulation and turbulent interaction regions near 11 AU, *J. Geophys. Res.*, *90*, 12,017, 1985.
Burlaga, L. F., M. L. Goldstein, F. B. McDonald, A. J. Lazarus, F. Mariani, F. M. Neubauer, and R. Schwenn, Cosmic ray variations and turbulent flow systems: 0.3–1.0 AU; 1977–1980, *J. Geophys. Res.*, *91*, 2917, 1986.
Burlaga, L. F., F. B. McDonald, and N. F. Ness, Cosmic ray modulation and the distant heliospheric magnetic field: Voyager 1 and 2 observations from 1986 to 1989, *J. Geophys. Res.*, *98*, 1, 1993.
Cane, H. V., Cosmic ray decreases and magnetic clouds, *J. Geophys. Res.*, *98*, 3509, 1993.
Cane, H. V., and I. G. Richardson, Cosmic ray decreases and solar wind disturbances during late October 1989, *J. Geophys. Res.*, *100*, 1755, 1995.
Cane, H. V., I. G. Richardson, and T. T. von Rosenvinge, Cosmic ray decreases and particle acceleration in 1978–1982 and the associated solar wind structures, *J. Geophys. Res.*, *98*, 13,295, 1993.
Cane, H. V., I. G. Richardson, T. T. von Rosenvinge, and G. Wibberenz, Cosmic ray decreases and shock structure: A multi-spacecraft study, *J. Geophys. Res.*, *99*, 21,429, 1994.
Cane, H. V., I. G. Richardson, and G. Wibberenz, The response of energetic particles to the presence of ejecta material, *Proc. Int. Conf. Cosmic Rays 24th*, *4*, 377, 1995.
Couzens, D. A., and J. H. King, Interplanetary medium data book, Supplement 3, 1977–1985, *Rep. NSSDC/WDC-A 86-04*, Natl. Space Sci. Data Cent., Greenbelt, Md., 1986.
Duggal, S. P., and M. A. Pomerantz, Cosmic ray intensity variations associated with solar wind streams, *Proc. Int. Conf. Cosmic Rays 15th*, *3*, 370, 1977.
Duggal, S. P., B. T. Tsurutani, M. A. Pomerantz, C. H. Tsao, and E. J. Smith, Relativistic cosmic rays and corotating interaction regions, *J. Geophys. Res.*, *86*, 7473, 1981.
Forman, M. A., and L. J. Gleeson, Cosmic ray streaming and anisotropies, *Astrophys. Space Sci.*, *32*, 77, 1975.
Fujimoto, K., H. Kojima, K. Murakami, and K. Nagashima, IMF sector boundary and cosmic ray intensity variations, *Proc. Int. Conf. Cosmic Rays 17th*, *4*, 72, 1981.
Hamilton, D. C., The radial transport of energetic solar flare particles from 1 to 6 AU, *J. Geophys. Res.*, *82*, 2157, 1977.
Intriligator, D. S., and G. L. Siscoe, Stream interfaces and energetic ions closer than expected: Analyses of Pioneers 10 and 11 observations, *Geophys. Res. Lett.*, *21*, 1117, 1994.
Iucci, N., M. Parisi, M. Storini, and G. Villaresi, High speed solar wind streams and galactic cosmic ray modulation, I, *Nuovo Cimento Soc. Ital. Fis. C.*, *2*, 421, 1979.
Kota, J., and J. R. Jokipii, The role of corotating interaction regions in cosmic ray modulation, *Geophys. Res. Lett.*, *18*, 1979, 1991.
Kunow, H., M. Witte, G. Wibberenz, H. Hempe, R. Muller-Mellin, G. Green, B. Iwers, and J. Fuckner, Cosmic ray measurements on board Helios 1 from December 1974 to September 1975: Quiet time spectra, radial gradients, and solar events, *J. Geophys.*, *42*, 615, 1977.
Kunow, H., et al., High energy cosmic-ray nuclei results on Ulysses, 2, Effects of a recurrent high-speed stream from the southern polar coronal hole, *Space Sci. Rev.*, *72*, 397, 1995.
Lockwood, J. A., An investigation of the Forbush decreases in the cosmic radiation, *J. Geophys. Res.*, *65*, 3859, 1960.
Lockwood, J. A., W. R. Webber, and H. Debrunner, The rigidity dependence of Forbush decreases observed at the Earth, *J. Geophys. Res.*, *96*, 5447, 1991.
Lopez, R. E., Solar cycle invariance in solar wind proton temperature relationships, *J. Geophys. Res.*, *92*, 11,189, 1987.
McCracken, K. G., U. R. Rao, and R. P. Bukata, Recurrent Forbush decreases associated with M-region magnetic storms, *Phys. Rev. Lett.*, *17*, 928, 1966.
McGuire, R. E., T. T. von Rosenvinge, and F. B. McDonald, The composition of solar energetic particles, *Astrophys. J.*, *301*, 938, 1986.
Mishra, B. L., and S. P. Agrawal, Study of dominating parameters of high speed solar plasma streams in relation to cosmic ray and geomagnetic storms, *Proc. Int. Conf. Cosmic Rays 19th*, *5*, 254, 1985.
Mishra, B. L., P. K. Shrivastava, and S. P. Agrawal, Spectral signatures of two types of solar wind streams on cosmic ray intensity during 1979–86, *Proc. Int. Conf. Cosmic Rays 21st*, *6*, 299, 1990.
Morfill, G., A. K. Richter, and M. Scholer, Average properties of cosmic ray diffusion in solar wind streams, *J. Geophys. Res.*, *84*, 1505, 1979.
Morfill, G., M. Scholer, and M. A. I. Van Hollebeke, The longitudinal galactic cosmic ray intensity modulation in a diffusive and scatter-free model of the inner heliosphere, *J. Geophys. Res.*, *85*, 2307, 1980.
Müller-Mellin, R., and G. Wibberenz, Energetic particles at high latitudes, *Space Sci. Rev.*, *72*, 273, 1995.
Murayama, T., K. Maezawa, and K. Hakamada, Time profiles of Forbush decreases and their relation to the structure of the interplanetary magnetic field, *Conf. Pap. Int. Cosmic Ray Conf. 16th*, *3*, 416, 1979.
Newkirk, G., Jr., and L. A. Fisk, Variation of cosmic rays and solar wind properties with respect to the heliospheric current sheet, 1, Five-GeV protons and solar wind, *J. Geophys. Res.*, *90*, 3391, 1985.
Richardson, I. G., Low energy ions in co-rotating interaction regions at 1 AU: Evidence for statistical ion acceleration, *Planet. Space Sci.*, *33*, 557, 1985.
Richardson, I. G., and H. V. Cane, Corotating >60 MeV/amu cosmic ray depressions observed by spacecraft anti-coincidence guards, *Proc. Int. Conf. Cosmic Rays 24th*, *4*, 960, 1995a.
Richardson, I. G., and H. V. Cane, Regions of abnormally low proton temperatures in the solar wind (1965–1991) and their association with ejecta, *J. Geophys. Res.*, *100*, 23,397, 1995b.
Schwenn, R., Large-scale structure of the interplanetary medium, in *Physics of the Inner Heliosphere*, vol. 1, edited by R. Schwenn and E. Marsch, P. 99, Springer-Verlag, New York, 1990.
Shrivastava, P. K., and R. P. Shukla, Effects of two types of high speed solar wind streams on cosmic ray intensity and on geomagnetic disturbance, *Proc. Int. Conf. Cosmic Rays 23rd*, *3*, 489, 1993.
Singh, R. L., D. P. Tiwari, and S. K. Nigam, Long lasting equatorial coronal holes and 27 days recurrence tendency in cosmic radiation, *Proc. Int. Conf. Cosmic Rays 21st*, *6*, 295, 1990.
Smith, E. J., and J. Wolfe, Pioneer 10, 11 observations of evolving solar wind streams and shocks beyond 1 AU, in *Study of Travelling Interplanetary Phenomena*, edited by M. A. Shea et al., p. 227, D. Reidel, Norwell, Mass., 1977.
Tiwari, D. P., R. P. Mishra, A. P. Mishra, and R. L. Singh, Solar wind stream interfaces and transient decreases in cosmic ray intensity, *Proc. Int. Conf. Cosmic Rays 18th*, *3*, 221, 1983.
Tsurutani, B. T., C. M. Ho, J. K. Arballo, B. E. Goldstein, and A. Balogh, Large-amplitude IMF fluctuations in corotating interaction regions: Ulysses at midlatitudes, *Geophys. Res. Lett.*, *22*, 3397, 1995.
Van Hollebeke, M. A. I., F. B. McDonald, and T. T. von Rosenvinge, The radial variation of corotating energetic particle streams in the inner and outer solar system, *J. Geophys. Res.*, *83*, 4723, 1978.
Venkatesan, D., A. K. Shukla, and S. P. Agrawal, Cosmic ray intensity variations and two types of high-speed solar wind streams, *Sol. Phys.*, *81*, 375, 1982.
Wanner, W., and G. Wibberenz, A study of the propagation of solar energetic protons in the inner heliosphere, *J. Geophys. Res.*, *98*, 3513, 1993.

H. V. Cane and I. G. Richardson, Laboratory for High Energy Astrophysics, NASA Goddard Space Flight Center, Code 661, Greenbelt, MD 20771. (e-mail: cane@nssdca.gsfc.nasa.gov; richardson@1heavx.gsfc.nasa.gov)

G. Wibberenz, Institut für Reine und Angewandte Kernphysik, Universität Kiel, 24118 Kiel, Germany. (e-mail: ifkki::wibberenz)

(Received November 9, 1995; revised February 14, 1996;
accepted February 15, 1996.)